Inverse Rectification in Donor–Acceptor Molecular Heterojunctions

Shannon K. Yee,[†] Jibin Sun,[‡,§] Pierre Darancet,[⊥] T. Don Tilley,[§] Arun Majumdar,[∥] Jeffrey B. Neaton,[⊥,*] and Rachel A. Segalman[‡,*]

[†]Department of Mechanical Engineering, [‡]Department of Chemical and Biomolecular Engineering, and [§]Department of Chemistry, University of California, 201D Gilman Hall, Berkeley, California 94720-1462, United States, [⊥]Molecular Foundry, Lawrence Berkeley National Laboratory, Berkeley, California 94720, United States, and [∥]U.S. Department of Energy, ARPA-E, Washington, DC 20585, United States

ABSTRACT The transport properties of a junction consisting of small donor–acceptor molecules bound to Au electrodes are studied and understood in terms of its hybrid donor–acceptor–electrode interfaces. A newly synthesized donor–acceptor molecule consisting of a bithiophene donor and a naphthalenediimide acceptor separated by a conjugated phenylacetylene bridge and a nonconjugated end group shows rectification in the reverse polarization, behavior opposite to that observed in mesoscopic p–n junctions. Solution-based spectroscopic measurements demonstrate that the molecule retains many of its original constituent properties, suggesting a weak hybridization between the wave functions of the donor and acceptor moieties, even in the presence of a conjugated bridge. Differential conductance measurements for biases as high as 1.5 V are reported and indicate a large asymmetry in the orbital contributions to transport arising from disproportionate electronic coupling at anode–donor and acceptor–cathode interfaces. A semi-empirical single Lorentzian coherent transport model, developed from experimental data and density functional theory based calculations, is found to explain the inverse rectification.

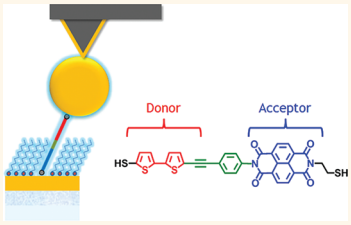

KEYWORDS: molecular diode · inverse rectification · donor–acceptor molecule · single-molecule conductance

In the pursuit of organic electronics,[1] better performance can be obtained by improving the transport properties at the anode–donor, donor–acceptor, and acceptor–cathode interfaces. Within a conventional bulk heterojunction photovoltaic device, these types of interfaces are present in extreme numbers, with significant variation, and are nearly impossible to characterize. A single acceptor–donor molecule covalently bound to electrodes including all three of these interfaces may be used as a model to understand interfacial transport in the context of a metal–molecule–metal heterojunction. In a pioneering study more than three decades ago, Aviram and Ratner first proposed that donor-σ-acceptor molecules might behave like diodes.[2] In recent years, measuring transport in single-molecule junctions[3] has become possible with advances in nanoscale manipulation, and the conductance of several molecular junctions[4] has been investigated. Since then, suggestions that light can couple with molecular heterojunctions[5,6] has rekindled interest in molecular diodes, or molecules with rectifying behavior.[7,8] Conductance measurements observing rectification have been performed on self-assembled monolayers (SAMs)[9−16] and in single-molecule junctions.[17−20] Furthermore, inverse rectification has also been theoretically predicted[21] where it is argued that asymmetric coupling of the molecule to the electrodes is primarily responsible for the inverse affect. In addition to asymmetric molecules, rectification has been reported in symmetric molecules where the electrode material varied.[17,19] In single-molecule measurements, scanning tunneling microscope (STM) break junctions, conducting atomic force microscopes (CAFMs), mechanically controlled break junctions, cross-wires, and electromigrated break junctions are common tools.[22] Of these techniques, CAFM has the benefit of using force as the feedback mechanism, decoupling the electrical measurement from the control mechanism.

RESULTS AND DISCUSSION

Herein, we report our observations of a newly synthesized molecule consisting of a bithiophene donor and a naphthalenediimide acceptor separated by a phenylacetylene bridge (bithiophene–phenylacetylene–naphthalenediimide–dithiol (BPNDT); Figure 1); synthetic details are available in the Supporting Information. Transport measurements

* Address correspondence to segalman@berkeley.edu, jbneaton@lbl.gov.

Received for review September 13, 2011 and accepted October 19, 2011.

Published online October 19, 2011
10.1021/nn203520v

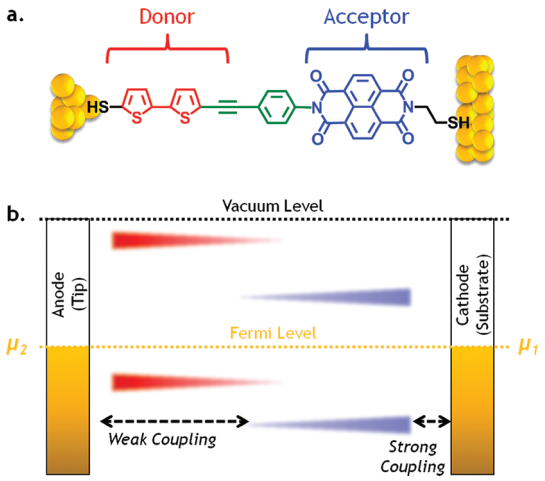

Figure 1. Simplified energy level diagram of the metal–molecule–metal heterojunction. (a) Structure of the junction: the molecule is connected to the anode (tip) and to the cathode (substrate) through thiol binding groups. The bridge (green) breaks the conjugation of the wave functions between the donor and acceptor parts of the molecule. (b) Schematics of the expected local density of states (LDOS). The states under the Fermi level are occupied. Due to the bridge and their localization on one side of the molecule, the molecular levels are more coupled to one side of the junction.

are carried out using a modified CAFM technique previously developed by Morita *et al.*[23] A SAM of decanethiol is initially created on a smooth conducting substrate using a mechanically stripped silicon template technique.[24−26] We obtain near atomically flat substrates with an rms roughness of 1.68 ± 0.18 Å over a scan area of 50 × 50 nm. After the formation of the SAM in a decanethiol solution, the BPNDT molecules were inserted into the defects of that SAM again using a solution-based self-assembly. In this step, the BPNDT molecule has a trimethylsilyl (TMS) group protecting the thiol closest to the donor. Since only one thiol bonding group (closest to the naphthalenediimide) is exposed, the molecule will preferentially orient itself with the acceptor bound to the substrate. Upon bonding to the substrate, the protecting TMS group is removed using a solution of tetra-*n*-butylammonium fluoride, exposing a free thiol pointing up away from the substrate. The substrate is then placed in a solution of 5 nm Au nanoparticles (NPs) allowing the unprotected end of BPNDT to covalently bond to a NP. Au NPs are synthesized[23,27] and coated with *n*-tetraoctlyammonium bromide ligands. It is believed that the thiol–Au bond is stronger than the ligand–Au bond, and it is expected that BPNDT will displace the ligand,[23] allowing the NP to become anchored to the BPNDT. As a final step, contact is made to the NP using a CAFM. This entire preparation process is summarized in Figure 2 (details in the Supporting Information).

Figure 3 consists of a sequence of AFM images taken after each phase of assembly described in Figure 2. The SAM survives the assembly, and BPNDT molecules appear to have preferentially attached at the SAM grain boundaries, consistent with the expectation that BPNDT binds strongest to SAM defects. After removing the TMS protection group, the AFM image sharpness is reduced, attributed to free thiols interacting with the AFM tip. (When exposed thiol bonding groups are not present, the NPs do not bond to the surface, as shown in Figure 3e.) A number of 5 nm Au NPs are observed. Lateral AFM tip broadening (tip radius ∼30 nm) depicts the NPs as being larger (∼60 nm) than 5 nm; however, the size of the NP can be confirmed using the vertical color bar. While this self-assembly contains multiple steps, it can produce repeatable results with areal control using solution processes for longer molecules—such as BPNDT—that protrude above the host SAM and that do not naturally form an ordered monolayer.

When the AFM tip is in contact with the NPs, thermal drift presents a challenge in creating reproducible and controllable measurement. To overcome this, several tapping (AC) images of the NP surface are captured prior to contact. Between sequential images, a built-in image comparison program is used to analyze the images and determine the lateral drift rates. The lateral piezoactutators are then ramped to follow these drift rates. Using this drift compensation routine, NPs on the image remain fixed to within the tip radius (*i.e.*, no perceptible movement) over hour time scales at room temperature operation. Sets of five NPs are visually selected for contact from these images. Automated contact to each of the NPs is made with a force of 7–13 nN. Upon contact to each NP, 10 trianglular current–voltage (*IV*) sweeps are carried out at a sweep rate of 20 kHz to minimize the capacitive ($C \sim 10$ pF) hysteresis of $I = C dV/dt$ between the cantilever and the substrate. The average of these 10 sweeps is then taken as the *IV* trace for that molecular heterojunction. After completing the set, additional images of the surface are gathered to guarantee that the sample was not perturbed during contact. Sets that visually showed alternations (*e.g.*, Au flaking from the AFM tip) are excluded from analysis. In this manner, ∼75 molecular heterojunctions spanning three separate samples are analyzed.

IV characteristics obtained from a sample junction are shown in Figure 4a; larger currents are seen to be present under negative bias. Since the TMS group protects the thiol bonded to the donor, the molecular orientation is controlled so that the acceptor binds to the substrate, and the NP (and tip) makes contact with the donor. This orientation control, built directly into the synthesis of the molecule, allows the unambiguous definition of *forward* bias as *positive* voltages in which the tip is biased relative to the substrate. Under forward bias, the chemical potential of the substrate is greater than that of the tip, and electrons flow from substrate to tip. Interestingly, the molecular junction

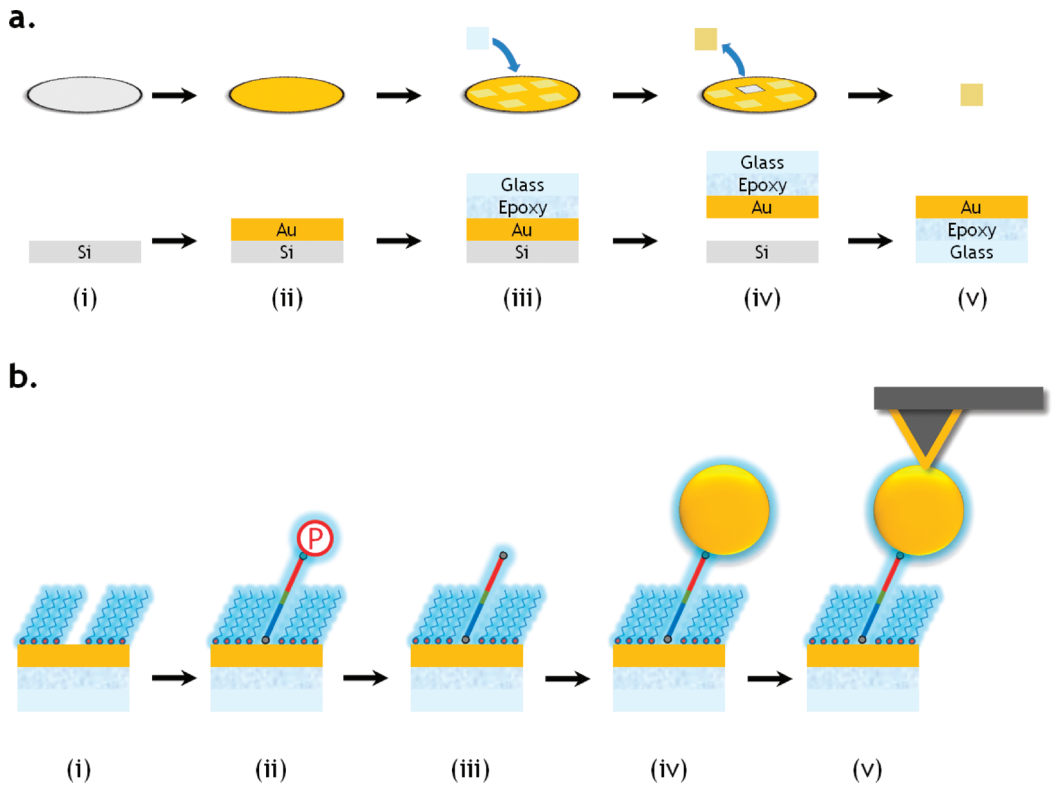

Figure 2. (a) Substrate preparation: (i) silicon wafer acts as a template where (ii) 200 nm of Au is sputtered onto the surface. (iii) Next, an epoxy-coated glass microscope cover slide is placed directly onto the Au and allowed to cure. (iv) Substrate is mechanically cleaved from the silicon template exposing a (v) fresh, nearly atomically smooth, Au surface. (b) Sample preparation: (i) SAM of decanethiols forms on the Au surface in a toluene solution. (ii) In another toluene solution, the donor–acceptor molecule directionally inserts into the defects of the SAM since only one bonding group is exposed. (iii) Protection group is removed in a separate toluene solution process, and then the substrate is immersed in a toluene solution of Au NPs (iv) which then bind to the newly exposed binding group of the donor–acceptor molecule. (v) Finally, a Au-coated AFM cantilever contacts the Au NP forming a metal–molecule–metal heterojunction (see Supporting Information for details).

exhibits higher conductance under a reverse (negative) bias, with electrons flowing opposite to the molecular dipole moment. Evidently, the electrons flow from the tip through the donor, then the acceptor, and into the substrate. This behavior is opposite to that of a macroscopic p–n junction, where more current (and enhanced conductance) is observed when electrons flow from the n-type semicoductor (acceptor analogue) through the p-type material (donor analogue). Similar to diodes however, asymmetric *IV* traces with the same polarity are present in every molecular junction.

Taking the *IV* traces from each heterojunction, the rectifying behavior and the differential conductance (dI/dV) of these systems can be explored further. A rectification ratio, RR, is defined as the positive ratio of currents of the *IV* traces at various positive and negative bias voltages, V

$$\mathrm{RR}(V) = \frac{-I(-V)}{I(V)} = \frac{-I_{\mathrm{reverse}}}{I_{\mathrm{forward}}}$$

The RR is determined for every sweep for several values of V and then histogrammed, which is represented by the color map in Figure 4c. Since each heterojunction may be different (*e.g.*, molecular orientation, contact, *etc.*), we determine the RR for each heterojunction. The RR obtained from the average *IV* is nevertheless similar. The RR value appears to increase with increasing bias and crosses a RR = 1 threshold around 0.6 V, which is consistent with the shape of the characteristic *IV* trace in Figure 4a. While the rectification ratio is small, which suggests that this is a weak molecular diode, under biases greater than 1 V, all heterojunctions appear to have a RR > 1. At 1 V, the average RR is 1.2 and appears to increase at higher biases. As defined, RR > 1 suggests that the rectification is opposite that of semiconductor diodes based on p–n junctions, where the RR would be defined as the ratio of the forward to reverse bias current (which for p–n diode would be strictly <1). This suggests that the direct analogue to p–n diodes is inappropriate for these single-molecule rectifiers, and another description is necessary.

To gain insight into the electronic structure of junction, we examine the gas- and solution-phase spectroscopy of BPNDT using a combination of theory and experiment. Density functional theory (DFT) calculations are performed to explore the spatial character of

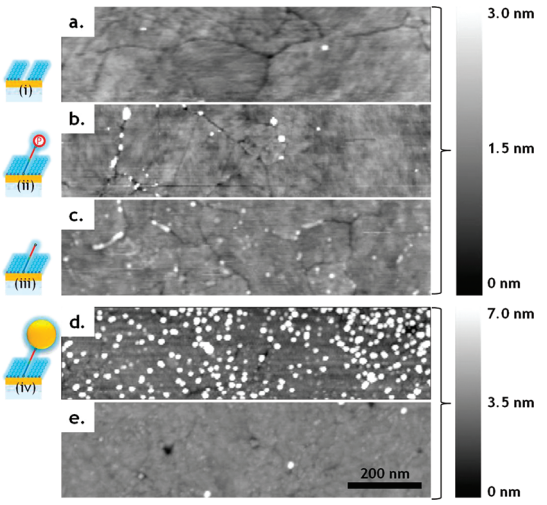

Figure 3. AFM images of sample surface at different stages of the molecular assembly process. Images are acquired in tapping mode (*i.e.*, AC mode) interacting with attractive forces between the tip and the sample. The length scale bar is the same for all images, but the color bar is only common to a−c and common to d,e. (a) DeT SAM on Au substrate; large grain boundaries are visible. (b) DeT SAM after allowing protected P−N molecules to bind in SAM defects. Large agglomerations appear to concentrate on grain boundaries. (c) DeT SAM and donor−acceptor molecules after protection groups are removed. Large agglomerations still appear at grain boundaries. Images tend to appear slightly less sharp, and it is speculated that the exposed thiol end groups interact more strongly with the AFM tip causing blurring. (d) NPs adhere to the surface *via* exposed thiol bonds even after a vigorous rinse. The AFM tip broadening artifact is observed, but the color bar confirms the size of NPs. (d) DeT SAM immersed in NP solution and then rinsed; Au NPs do not appear to adhere to the sample because there are no exposed thiols.

the frontier orbitals of BPNDT molecule with thiol end groups (see Supporting Information for calculation details). Figure 5 shows the last few occupied and first few unoccupied orbitals computed with DFT. The hybridization between the donor and acceptor moieties is quite limited: the highest occupied molecular orbital (HOMO) lies principally on the donor (*i.e.*, bithiophene), with negligible weight on the acceptor (*i.e.*, naphthalenediimide), and strongly hybridizes with the thiol end group. Strong spatial localization on either the donor or acceptor and weak hybridization across the bridge are observed for the other frontier orbitals, as well: the lowest unoccupied molecular orbital (LUMO) sits on the acceptor, and LUMO+1 sits again on the acceptor. The HOMO-1 orbital is entirely localized on the thiol end group on the acceptor side, and thus it in particular would not be expected to affect junction transport properties. Observing that all frontier orbitals are spatially localized to one side of the molecule lends strong support to the simplified level diagram in Figure 1.

Comparisons of UV−vis spectra of BPNDT in solution (Figure 4b) support a picture of weak hybridization between donor and acceptor states in these molecules. A broad peak in BPNDT's absorption spectrum is present at 3.4 ± 0.3 eV, similar to the naphthalenediimide constituent's absorption maxima at 3.3 ± 0.1 and 3.5 ± 0.1 eV. Emission spectra are collected upon excitation at 3.80 ± 0.02 eV, and increasing the excitation frequency results in negligible change in the spectra. A single peak in the BPNDT's emission spectrum at 2.7 ± 0.3 eV closely resembles that of naphthalenediimide with a small blue shift. (The smaller peaks Figure 4b at 325 and 650 nm are harmonics of the excitation.) The absorption peak of the donor constituent at ~4.1 eV is absent in the combined molecule, consistent with the DFT calculations which showed that the HOMO of the donor is strongly affected by the presence of the end group. Further, once hybridized with the phenylacetylene bridge and the thiol end group, and in the presence of solvent, the donor moiety absorption would be expected to red shift, resulting in an absorption peak on the donor side indistinguishable from the broad acceptor peak. Newly available "charge transfer" states, resulting from the HOMO of the donor and the LUMO of the acceptor, would be expected to appear at low energy in the absorption or emission spectra. The lack of an absorption or emission significantly red-shifted suggests that such states have an extremely weak optical cross section, resulting from a negligible overlap and a corresponding negligible dipole transition matrix. With these measurements and DFT calculations, we conclude that the phenylacetylene bridge moiety effectively decouples the donor and acceptor molecular orbitals.

Given the spectroscopy and DFT calculations above, a hypothesis of the junction electronic structure is posed, as shown in Figure 1. With this junction electronic structure, a straightforward single-Lorentzian Landauer expression for the current−voltage characteristic, coupled with the DFT calculations and solution-phase spectroscopy, can explain the measured transport data. In the Landauer formalism, charge carriers tunnel coherently through the junction with an energy-dependent probability given by the transmission function, τ. Neglecting inelastic scattering events, and assuming that the tunneling is fast compared with typical vibration frequencies, the current I_{1-2} induced by an applied bias V_{1-2} between electrode 1 and electrode 2 is given by

$$I(V_{1-2}) = \mathrm{sign}(V_{1-2})G_0 \int_{-|V_{1-2}|/2}^{+|V_{1-2}|/2} \tau(\omega, E(V_{1-2}))\mathrm{d}\omega \quad (1)$$

where $G_0 = 2e^2/h$ is the quantum of conductance and ω is the energy of the electron participating in transport through a single bias-dependent resonance level $E(V_{1-2})$. If we consider the case of well-separated molecular energy levels, one can write the

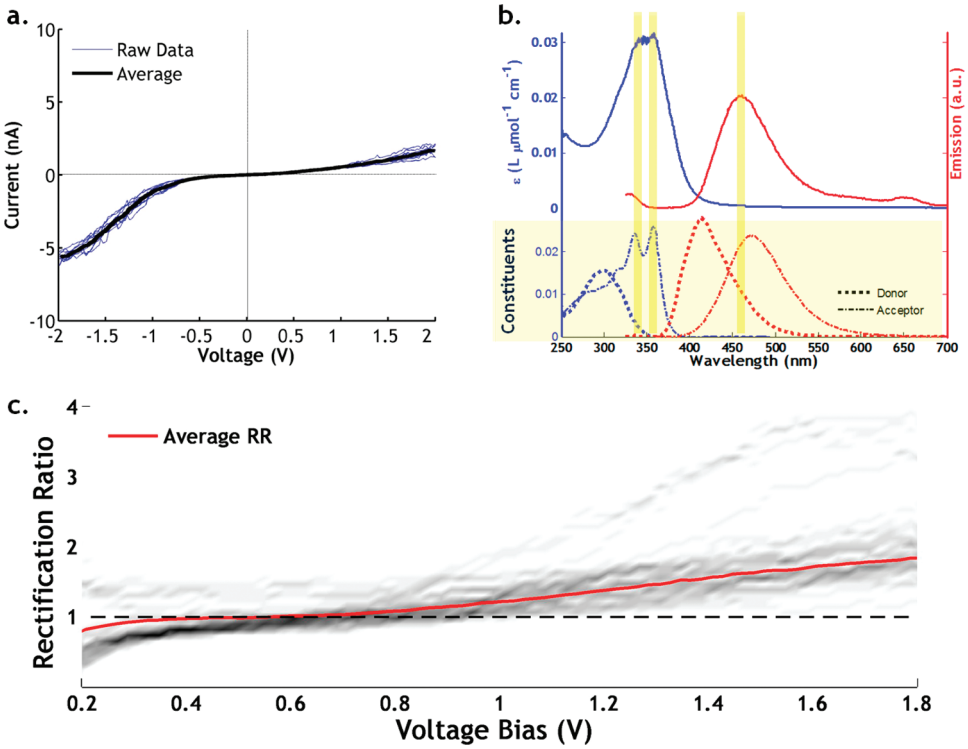

Figure 4. (a) Characteristic *IV* curve of a metal–molecule–metal junction showing the average *IV* curve over 10 traces. Asymmetry in the *IV* curve is visible and agrees with polarity predicted in theory. (b) Absorption (blue) and emission (red) spectra of donor–acceptor molecule (top) and of constituent molecules (bottom) in toluene. The donor–acceptor molecule has spectral characteristics that are most similar to the acceptor constituent spectrum which exhibits two absorption peaks. (c) Average rectification ratio (red) and underlying color map depicting the rectification ratio distribution of individual junctions.

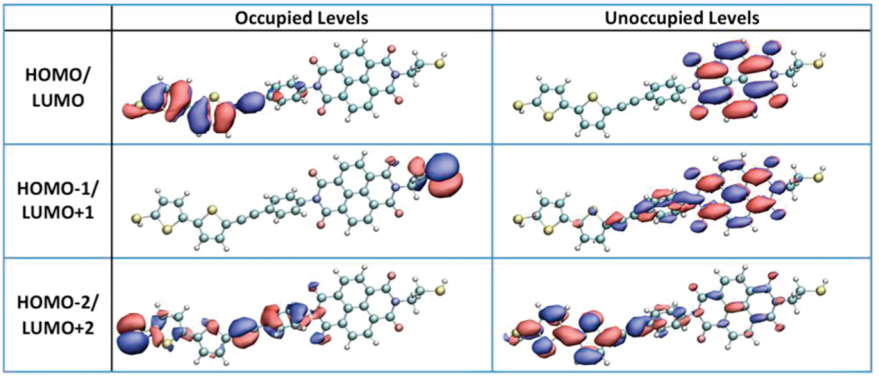

Figure 5. Gas-phase DFT calculations depicting the localization of molecular orbitals around the bithiophene donor or naphthalene acceptor. This depiction suggests that the wave functions weakly overlap and that the molecule should exhibit rectifying behavior.

transmission function as

$$\tau(\omega, E(V_{1-2})) = \frac{4\lambda\Gamma^2}{(1+\lambda)^2\Gamma^2 + 4(\omega - E(V_{1-2}))^2} \quad (2)$$

where the coupling of the level to the closest lead is given by Γ and to the furthest lead by $\lambda\Gamma$ where, by convention, $\lambda < 1$.

The energy gap within the molecule will determine much of its transport characteristics. The computed gas-phase energy gap or difference between ionization potential and electron affinity—which refers to the removal or addition of an electron—is 4.49 eV for BPNDT (see Table 1). Computed energy gaps of the thiol-donor-bridge and acceptor-thiol moieties are 6.61 and 6.10 eV, respectively, and imply a gas-phase level offset between the donor HOMO and acceptor HOMO of around 1.5 eV. Upon junction formation, we expect that the gap will be further reduced by static polarization from the metal electrodes.[28] Using an electrostatic "image charge" estimate and different molecule–electrode geometries (see Supporting Information), we expect that

TABLE 1. ΔSCF Results for the Isolated Fragments and the Complete Molecule[a]

	ionization potential (eV)	electron affinity (eV)	energy gap (eV)
donor fragment	7.42	0.81	6.61
acceptor fragment	8.63	2.50	6.13
complete molecule	7.04	2.55	4.49

[a] The calculations for the donor fragments were done separating the molecule in two parts and passivating the end with hydrogen. The donor fragment then consists of the thiol end group coupled to the bithiophene and the phenylacetylene bridge; the acceptor fragment consists of the naphthalenediimide and a thiol end group. All calculations were performed using the software Qchem, with the energy of the relaxed structures given by B3LYP approximation on the exchange and correlation.

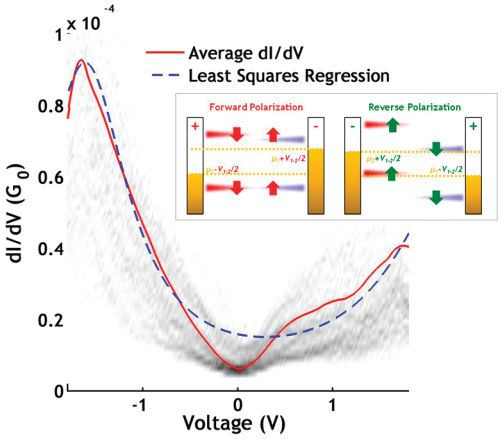

Figure 6. Average differential conductance d*I*/d*V* of the molecule (red) and the underlying color map corresponds to histograms fit to the experimental data of the one level model (blue). Inset: Schematics of the local density of states under finite bias. Due to the electric field present in the junction at finite bias, the energy of the levels changes as a function of their coupling with the leads. The forward polarization tends to reduce the intramolecular dipole and pulls the levels out of the bias window (yellow dashed line). The reverse polarization increases the intramolecular dipole and pushes the HOMO inside the bias window.

electrode polarization narrows the gap by about 0.8 eV. Furthermore, cyclic voltammetry measurements of BPNDT in solution with a Pt electrode (similar work function to Au) would place the HOMO's energy 1.4 eV below the Fermi level. This suggest that, with the ±2 V bias window, at most one resonant level ~2 eV from the Fermi level will be observed, substantiating the hypothesis of a single transmission channel. Furthermore, if this resonant energy level is bias-dependent, then the applied bias will force this resonant channel either into or away from the bias window, resulting in a rectifying behavior opposite of the expected mesoscopic behavior of a p−n junction. In this case, direct but highly asymmetric coupling between both electrodes and each of the MOs is present, and rectification can be explained by a single bias-dependent frontier orbital energy level.

To validate this picture, the numerical derivative of individual *IV* characteristics is performed to produce differential conductance traces. Histograms of these traces taken at discrete voltages are created and illustrated in a color map in Figure 6. Below, we develop a minimal physical model that can explain the differential conductance experimental data and inverse rectification. We assume a linear dependence of the resonant transmission level with bias

$$E(V_{1-2}) = \frac{\alpha}{2}V_{1-2} + E_0 \tag{3}$$

where E_0 represents the position of the molecular orbital at zero bias and $\alpha = \pm 1$ corresponds to the level moves rigidly with the chemical potential of an electrode (Tersoff−Hamann limit), while $\alpha = 0$ indicates that the energy of the molecular orbital is bias-independent. Next, the differential conductance can be expressed, in this simple Landauer picture, as

$$\left.\frac{dI(V)}{dV}\right|_{V=V_{1-2}} = 2G_0\lambda\Gamma^2\left[\frac{1+\alpha}{\Gamma^2+4\left(E_0+\frac{V_{1-2}}{2}\times(1+\alpha)\right)^2} + \frac{1-\alpha}{\Gamma^2+4\left(-E_0+\frac{V_{1-2}}{2}\times(1-\alpha)\right)^2}\right] \tag{4}$$

This expression provides a good fit to the average differential conductance with the parameters: $\alpha = -0.19$, $\lambda = 3.8 \times 10^{-5}$, $\Gamma = 1.31$ eV, and $E_0 = -1.9$ eV. Consistent with expectations, the molecular orbital energy is below the Fermi level, indicating that the transmission is dominated by the HOMO, and the field moves the HOMO with ~20% efficiency, in line with the computed dipole matrix element in the gas phase; the ratio λ between the strongly and weakly coupled leads is $\sim 10^{-5}$, which follows from the strong spatial separation of the HOMO and LUMO computed from DFT. Thus overall, this fit is highly consistent with our DFT calculations, spectroscopy experiments, and electrochemical measurements on BPNDT.

Most importantly, the coherent tunneling model described above provides an explanation of the inverse rectification. From Figure 1, the reverse polarization drives the HOMO of the donor toward the bias window, and the forward polarization pushes it away from the bias window, resulting in a larger current for reverse bias, as experimentally observed. The magnitude of the current is tied to the position of the resonance energy E_0 and coupling Γ; the level energy E_0 must be close enough to the Fermi level and the coupling Γ must be large enough to yield observable current. The low peak height ($\ll 1$) at resonance is rigorously connected to the small λ associated with the donor's HOMO being much more strongly coupled

to the NP than to the substrate. This picture of transport suggests that rectifying behavior of BPNDT originates, in this case, with the strength and asymmetry of the orbital coupling and the alignment of orbital energies with the junction Fermi level.

CONCLUSION

In summary, a newly synthesized molecule constructed from a bithiophene donor, naphthalenediimide acceptor, and phenylacetylene bridge is demonstrated to operate as a bipolar molecule. By a robust self-assembling CAFM technique, this molecule exhibits rectification over a wide range of voltages. A simple single-level coherent tunneling model was able to explain the differential conductance and rectification, suggesting both are highly sensitive to the position of the level relative to the contact Fermi level and the strength of orbital–electrode coupling and its asymmetry. This work further suggests that a suite of molecules can be synthesized to further explore connections between junction electronic structure and rectification.

METHODS

Au NPs were carefully synthesized following similar procedures previously reported in literature,[23,27] and details are reproduced in the Supporting Information. Au substrates were prepared using the template-stripped gold technique previously reported in literature,[24–26] and details are reproduced in the Supporting Information. The AFM tips were modified from commercially available Olympus AC240TS silicon AFM cantilevers (spring constant ~2 N/m, tip radius ~9 nm) following the procedure outlined by Morita.[23] The P–N molecules were synthesized in-house, and a detailed description is found in the Supporting Information. Samples were prepared by immersing a freshly stripped Au substrate in a 0.1 mM decanethiol anhydrous toluene solution for 5 h. Next, the substrate was rinsed with anhydrous toluene and immersed in a 0.1 mM P–N molecule anhydrous toluene solution for 12 h. Again, the substrate was rinsed with anhydrous toluene and then immersed in an anhydrous ethanol solution of tetra-*n*-butylammonium fluoride (TBAF) for 1 h. This removed the protection group and exposed a thiol end group. Next, the substrate was rinsed in anhydrous ethanol and then immersed in a toluene solution containing the Au NP for 30 min. The NP solution was added dropwise to toluene until the UV–vis absorption optical density (o.d.) in a 1 cm cuvette was ~0.2 at the plasmon resonance peak (approximately 0.1 mL of NP solution in 10 mL of toluene). The substrate was thoroughly rinsed one final time with anhydrous toluene, stored under N_2 for transport, and then measured immediately in the AFM chamber and measured as discussed in the Results and Discussion section using an Asylum MFP3D AFM. Solid-state data analysis was performed on 77 junctions from three separate samples (*i.e.*, 26, 27, and 24 junctions in each sample). The ~5% of junction acquired (not included in the previous tally) had traces with either (i) zero current or (ii) saturated current attributed to a situation where (i) a metal–molecule–metal junction was not formed or (ii) a short between the tip and substrate occurred due to AFM snap-in; these traces were excluded from analysis. All measured molecular junctions, however, showed the same reverse rectification behavior suggesting a high yield on the orientation control.

Acknowledgment. This work was funded by the Helios Solar Energy Research Center, which is supported by the Director, Office of Science, Office of Basic Energy Sciences of the U.S. Department of Energy under Contract No. DE-AC02-05CH11231. We would also like to thank the Fannie and John Hertz Foundation for their fellowship support for S.Y. We are also extremely grateful for conversations with Peter Doak (LBNL), Jon Malen (CMU), and Pramod Reddy and his students Aaron Tan, Woochul Lee, Seid Sadat, and Won Ho Jeong (U. Mich).

Supporting Information Available: Nanoparticle synthesis, substrate preparation, AFM tip preparation, sample preparation, molecular synthesis, solid-state measurements, molecular calculations, and electronic transport model. This material is available free of charge *via* the Internet at http://pubs.acs.org.

REFERENCES AND NOTES

1. Service, R. F. Breakthrough of the Year: Molecules Get Wired. *Science* **2001**, *294*, 2442–2443.
2. Quek, S. Y.; Venkataraman, L.; Choi, H. J.; Loule, S. G.; Hybertsen, M. S.; Neaton, J. B. Amine-Gold Linked Single-Molecule Circuits: Experiment and Theory. *Nano Lett.* **2007**, *7*, 3477–3482.
3. Aviram, A.; Ratner, M. A. Molecular Rectifiers. *Chem. Phys. Lett.* **1974**, *29*, 277–283.
4. Reed, M. A.; Zhou, C.; Muller, C. J.; Burgin, T. P.; Tour, J. M. Conductance of a Molecular Junction. *Science* **1997**, *278*, 252–254.
5. Venkataraman, L.; Klare, J. E.; Tam, I. W.; Nuckolls, C.; Hybertsen, M. S.; Steigerwald, M. L. Single-Molecule Circuits with Well-Defined Molecular Conductance. *Nano Lett.* **2006**, *6*, 458–462.
6. Xu, B. Q.; Tao, N. J. J. Measurement of Single-Molecule Resistance by Repeated Formation of Molecular Junctions. *Science* **2003**, *301*, 1221–1223.
7. Ward, D. R.; Halas, N. J.; Ciszek, J. W.; Tour, J. M.; Wu, Y.; Nordlander, P.; Natelson, D. Simultaneous Measurements of Electronic Conduction and Raman Response in Molecular Junctions. *Nano Lett.* **2008**, *8*, 919–924.
8. Wu, S. W.; Ogawa, N.; Ho, W. Atomic-Scale Coupling of Photons to Single-Molecule Junctions. *Science* **2006**, *312*, 1362–1365.
9. Wold, D. J.; Frisbie, C. D. Formation of Metal–Molecule–Metal Tunnel Junctions: Microcontacts to Alkanethiol Monolayers with a Conducting AFM Tip. *J. Am. Chem. Soc.* **2000**, *122*, 2970–2971.
10. Wold, D. J.; Haag, R.; Rampi, M. A.; Frisbie, C. D. Distance Dependence of Electron Tunneling through Self-Assembled Monolayers Measured by Conducting Probe Atomic Force Microscopy: Unsaturated *versus* Saturated Molecular Junctions. *J. Phys. Chem. B* **2002**, *106*, 2813–2816.
11. Dhirani, A.; Lin, P. H.; Guyot-Sionnest, P.; Zehner, R. W.; Sita, L. R. Self-Assembled Molecular Rectifiers. *J. Chem. Phys.* **1997**, *106*, 5249–5253.
12. Ashwell, G. J.; Tyrrell, W. D.; Whittam, A. J. Molecular Rectification: Self-Assembled Monolayers in Which Donor-Bridge-Acceptor Moieties Are Centrally Located and Symmetrically Coupled to Both Gold Electrodes. *J. Am. Chem. Soc.* **2004**, *126*, 7102–7110.
13. Nijhuis, C. A.; Reus, W. F.; Whitesides, G. M. Molecular Rectification in Metal–SAM–Metal Oxide–Metal Junctions. *J. Am. Chem. Soc.* **2009**, *131*, 17814–17827.
14. Chabinyc, M. L.; Chen, X.; Holmlin, R. E.; Jacobs, H.; Skulason, H.; Frisbie, C. D.; Mujica, V.; Ratner, M. A.; Rampi, M. A.; Whitesides, G. M. Molecular Rectification in a Metal–Insulator–Metal Junction Based on Self-Assembled Monolayers. *J. Am. Chem. Soc.* **2002**, *124*, 11730–11736.
15. Metzger, R. M. Electrical Rectification by a Molecule: The Advent of Unimolecular Electronic Devices. *Acc. Chem. Res.* **1999**, *32*, 950–957.

16. Metzger, R. M.; Xu, T.; Peterson, I. R. Electrical Rectification by a Monolayer of Hexadecylquinolinium Tricyanoquinodimethanide Measured between Macroscopic Gold Electrodes. *J. Phys. Chem. B* **2001**, *105*, 7280–7290.
17. Elbing, M.; Ochs, R.; Koentopp, M.; Fischer, M.; von Hanisch, C.; Weigend, F.; Evers, F.; Weber, H. B.; Mayor, M. A Single-Molecule Diode. *Proc. Natl. Acad. Sci. U.S.A.* **2005**, *102*, 8815–8820.
18. Metzger, R. M. Unimolecular Electronics and Rectifiers. *Synth. Met.* **2009**, *159*, 2277–2281.
19. Ng, M. K.; Lee, D. C.; Yu, L. P. Molecular Diodes Based on Conjugated Diblock Co-oligomers. *J. Am. Chem. Soc.* **2002**, *124*, 11862–11863.
20. Reichert, J.; Ochs, R.; Beckmann, D.; Weber, H. B.; Mayor, M.; von Lohneysen, H. Driving Current through Single Organic Molecules. *Phys. Rev. Lett.* **2002**, *88*, 176804.
21. Pan, J. B.; Zhang, Z. H.; Deng, X. Q.; Qiu, M.; Guo, C. The Transport Properties of D- Sigma−A Molecules: A Strikingly Opposite Directional Rectification. *Appl. Phys. Lett.* **2011**, *98*, 013503.
22. Malen, J. A.; Yee, S. K.; Majumdar, A.; Segalman, R. A. Fundamentals of Energy Transport, Energy Conversion, and Thermal Properties in Organic−Inorganic Heterojunctions. *Chem. Phys. Lett.* **2010**, *491*, 109–122.
23. Morita, T.; Lindsay, S. Determination of Single Molecule Conductances of Alkanedithiols by Conducting-Atomic Force Microscopy with Large Gold Nanoparticles. *J. Am. Chem. Soc.* **2007**, *129*, 7262–7263.
24. Hegner, M.; Wagner, P.; Semenza, G. Ultralarge Atomically Flat Template-Stripped Au Surfaces for Scanning Probe Microscopy. *Surf. Sci.* **1993**, *291*, 39–46.
25. Stamou, D.; Gourdon, D.; Liley, M.; Burnham, N. A.; Kulik, A.; Vogel, H.; Duschl, C. Uniformly Flat Gold Surfaces: Imaging the Domain Structure of Organic Monolayers Using Scanning Force Microscopy. *Langmuir* **1997**, *13*, 2425–2428.
26. Wagner, P.; Hegner, M.; Guntherodt, H. J.; Semenza, G. Formation and *In-Situ* Modification of Monolayers Chemisorbed on Ultraflat Template-Stripped Gold Surfaces. *Langmuir* **1995**, *11*, 3867–3875.
27. Cigang, X.; Xu, C.; Zalinge, H.; Pearson, J. L.; Glidle, A.; Cooper, J. M.; Cumming, D. R. S.; Haiss, W.; Yao, J.; Schiffrin, D. J.; Proupín-Pérez, M.; *et al.* A Combined Top-Down Bottom-Up Approach for Introducing Nanoparticle Networks into Nanoelectrode Gaps. *Nanotechnology* **2006**, *17*, 3333–3339.
28. Neaton, J. B.; Hybertsen, M. S.; Louie, S. G. Renormalization of Molecular Electronic Levels at Metal−Molecule Interfaces. *Phys. Rev. Lett.* **2006**, *97*, 216405.